المجلة الليبية للدراسات الأكاديمية المعاصرة (Libyan Journal of Contemporary Academic Studies)
LJCAS, eISSN: 5970-3005
Volume 4, Issue 2, 2026, Pages: 01-15

Evaluating Coating Adhesion Strength on Steel: Investigating the Impact of Distilled Water and Salt Solutions on Coating Performance

Abdelhamid Issa Hwwili [1], Hafed I. S. Abdulsalam [2], Sulayman Y. Sulayman [3]
[1,2] Department of Metallurgical and Materials Engineering, Faculty of Engineering, University of Ajdabiya, Ajdabiya, Libya
[3] Corrosion Protection Department, Inspection Group, Sirte Company, Libya
*Corresponding author: abdelhamid.issa@uoa.edu.ly

تقييم قوة التصاق الطلاءات الواقية على أسطح الفولاذ: دراسة تأثير الماء المقطر والمحاليل الملحية على أداء الطلاءات

عبدالحميد عيسى محمد حويلي [1]، حافظ ادريس صالح عبدالسلام [2]، سليمان يونس سليمان سعد [3]
[3،1] قسم هندسة المعادن والمواد، كلية الهندسة، جامعة أجدابيا، أجدابيا، ليبيا
[2] قسم الحماية من التآكل، مجموعة التفتيش، شركة سرت، ليبيا

Received: 12-04-2026; **Accepted:** 27-06-2026; **Published:** 15-07-2026

Abstract:

This study evaluates the adhesion strength and electrochemical performance of two industrial coatings—Sigmashield 880 (light) and Simcoe 350 (dark)—applied to steel substrates and exposed to distilled water and acidic salt solutions over a four-week period. Six steel samples were prepared and categorized into two experimental groups: one treated with a zinc (Zn) inhibitor and hydrochloric acid, and another exposed to distilled water without inhibitor. Weekly monitoring of pH and voltage was conducted to assess electrochemical activity, followed by standardized pull-off tests to quantify coating adhesion strength. Results demonstrated that uninhibited samples exhibited significantly higher voltage readings and lower pH values, indicating elevated corrosion activity. Conversely, Zn-inhibited samples maintained lower and more stable electrochemical responses. Adhesion strength values ranged from 5 to 9 MPa, with the dark coating (Simcoe 350) without inhibitor achieving the highest value (9 MPa), while the light coating with inhibitor recorded the lowest (5 MPa). The findings underscore that while Zn inhibitors enhance electrochemical stability, final adhesion performance depends on complex interactions between coating composition, inhibitor compatibility, and environmental exposure. This research provides practical insights for optimizing protective coating systems in marine and industrial environments.

Keywords: Coating adhesion strength; Steel substrates; Zn inhibitor; Corrosion resistance; Electrochemical monitoring; Pull-off test; Environmental degradation.

الملخص :

تقيّم هذه الدراسة قوة التصاق والأداء الكهروكيميائي لطلائين صناعيين، هما: سيجماشيلد 880 (الطلاء الفاتح) وسيمكو 350 (الطلاء الداكن)، والمطبقين على أسطح فولاذية، حيث عُرضت العينات للماء المقطر ومحاليل ملحية حمضية على مدى أربعة أسابيع. حُضّرت ست عينات فولاذية وقُسّمت إلى مجموعتين تجريبيتين: عُولجت المجموعة الأولى بمثبط الزنك (Zn) وحمض الهيدروكلوريك، بينما عُرِضت المجموعة الثانية للماء المقطر دون استخدام أي مثبط للتآكل. أُجري رصد أسبوعي لدرجة الحموضة (pH) وفرق الجهد الكهربائي لتقييم النشاط الكهروكيميائي، أعقبه إجراء اختبارات شد قياسية (Pull-off tests) لقياس قوة التصاق الطلاء كمياً. أظهرت النتائج أن العينات التي لم تُعالج بمثبط التآكل سجلت قراءات جهد كهربائي أعلى بكثير وقيماً أقل لدرجة الحموضة، مما يشير إلى نشاط تآكل متزايد. وفي المقابل، حافظت العينات المعالجة بمثبط الزنك على استجابات كهروكيميائية أقل وأكثر استقراراً. تراوحت قيم قوة الالتصاق بين 5 و9 ميجاباسكال، حيث حقق الطلاء الداكن (سيمكو 350) بدون مثبط أعلى قيمة التصاق (9 ميجاباسكال)، في حين سجل الطلاء الفاتح المعالج بمثبط التآكل أدنى قيمة (5 ميجاباسكال). وتؤكد هذه النتائج أنه على الرغم من أن مثبطات الزنك تعزز الاستقرار الكهروكيميائي، إلا أن أداء الالتصاق النهائي يعتمد على تفاعلات معقدة بين تركيب الطلاء، وتوافق المثبط، والظروف البيئية المعرض لها. يوفر هذا البحث رؤى عملية قيّمة لتحسين أنظمة الطلاء الواقية في البيئات البحرية والصناعية.

الكلمات المفتاحية: قوة التصاق الطلاء؛ الأسطح الفولاذية؛ مثبط الزنك؛ مقاومة التآكل؛ الرصد الكهروكيميائي؛ اختبار الشد (Pull-off test)؛ التدهور البيئي.

Copyright: © 2026 by the authors. Submitted for possible open access publication under the terms and conditions of the Creative Commons Attribution (CC BY) license (https://creativecommons.org/licenses/by/4.0/).

1. Introduction

Corrosion represents a pervasive and economically damaging phenomenon that severely compromises the structural integrity and service life of steel components across construction, maritime, and industrial sectors. The electrochemical degradation of steel in aggressive environments leads to material loss, accelerated maintenance cycles, and catastrophic structural failures if left unmitigated. Among the most widely adopted and cost-effective mitigation strategies is the application of organic protective coatings, which function as physical barriers to limit the diffusion of moisture, oxygen, and aggressive ions to the metal surface. However, the long-term protective efficacy of any coating system is fundamentally governed by its interfacial adhesion strength, which dictates resistance to delamination, blistering, and underfilm corrosion under environmental stressors [1].

The adhesion performance of industrial coatings is highly sensitive to substrate preparation, coating formulation, and exposure conditions. Environmental variables such as salinity, pH fluctuations, and ionic concentration can initiate interfacial degradation, leading to progressive bond failure. To counteract these effects, corrosion inhibitors such as zinc-based additives are frequently integrated into coating matrices or applied as pretreatments to suppress anodic dissolution and promote passive layer formation. Despite their widespread industrial use, the synergistic interactions between specific coating chemistries, inhibitor concentrations, and environmental media remain insufficiently standardized in practical field applications [2].

This study systematically evaluates the adhesion strength and electrochemical stability of two commercially utilized industrial coatings — Sigmashield 880 (light) and Simcoe 350 (dark) — applied to steel substrates and exposed to controlled aqueous environments. The experimental design specifically investigates the influence of a zinc (Zn) inhibitor, hydrochloric acid modulation, and coating color/composition on voltage and pH trends over a four-week immersion period. By correlating real-time electrochemical monitoring with post-exposure mechanical pull-off testing, the research aims to identify optimal coating-inhibitor-environment combinations that maximize durability [3].

The findings of this investigation are expected to provide actionable insights for coating selection protocols, standardized testing frameworks, and predictive maintenance models in corrosive industrial settings. Ultimately, bridging the gap between laboratory simulation and field-relevant performance will contribute to enhanced corrosion management strategies, reduced lifecycle costs, and extended structural reliability for steel infrastructure [4].

2. Literature Review

Recent advancements in protective coating technologies have emphasized the role of nanostructured and hybrid polymer systems in enhancing corrosion resistance. Studies have demonstrated that nanostructured formulations create dense, defect-free barrier layers that significantly reduce corrosion rates compared to conventional single-phase coatings, particularly in acidic and saline environments. These systems leverage nanoscale pore blocking and tortuous diffusion pathways to delay electrolyte penetration to the steel substrate [1]. The integration of nanoparticles such as SiO_2, TiO_2, and ZnO into epoxy matrices has been shown to improve both barrier performance and mechanical durability, although achieving uniform dispersion remains a critical processing challenge.

Substrate preparation and surface roughness have been consistently identified as critical determinants of coating adhesion strength. Research on mechanical abrasion, chemical cleaning, and controlled pretreatment protocols confirms that optimized surface topography enhances mechanical interlocking and chemical bonding at the metal-polymer interface. Inadequate surface preparation remains a primary cause of premature coating delamination, regardless of the inherent quality of the applied paint system [2]. Standards such as ISO 8501-1 provide visual reference benchmarks for surface cleanliness, while ISO 8502-series standards address invisible contaminants that may compromise long-term adhesion.

Environmental degradation factors, particularly ultraviolet (UV) radiation and prolonged moisture exposure, significantly accelerate coating aging through polymer chain scission, pigment fading, and loss of flexibility. Long-term field and accelerated laboratory evaluations reveal that hybrid and organic-inorganic composite coatings exhibit superior UV stability and water barrier properties, making them highly suitable for marine and coastal infrastructure where solar exposure and humidity are persistent [3]. Cyclic weathering tests combining UV, salt fog, and thermal cycling have become essential for realistic service life prediction.

The development of self-healing and smart coating systems has emerged as a transformative approach to extending coating lifespan. These advanced formulations incorporate microcapsules, shape-memory polymers, or pH-responsive inhibitors that autonomously repair micro-cracks and neutralize localized corrosion cells. While laboratory-scale results are highly promising, commercial scalability and cost-effectiveness remain active areas of investigation [4]. Recent work on encapsulated magnesium-based and cerium-based inhibitors demonstrates near-complete recovery of barrier properties after mechanical damage in accelerated tests.

Electrochemical characterization techniques, particularly potentiodynamic monitoring and impedance spectroscopy, have become indispensable for quantifying coating degradation kinetics. Voltage and pH measurements serve as reliable indirect indicators of anodic/cathodic activity, enabling early detection of coating failure before macroscopic defects become visible. Continuous monitoring protocols provide dynamic insights

Copyright: © 2026 by the authors. Submitted for possible open access publication under the terms and conditions of the Creative Commons Attribution (CC BY) license (https://creativecommons.org/licenses/by/4.0/).

into inhibitor depletion, barrier breakdown, and interfacial stability over time [5]. The integration of these techniques with equivalent circuit modeling allows quantitative extraction of coating resistance and capacitance, which correlate strongly with field performance.

Coating thickness, chemical compatibility, and thermal post-treatment have also been extensively studied for their impact on functional performance. Optimal thickness ensures uniform coverage without inducing internal stress cracking, while thermal curing of carbon-based and ceramic coatings consistently improves interfacial adhesion and electrical/chemical resistance. Inorganic and barrier coatings demonstrate exceptional performance in highly aggressive industrial atmospheres, particularly when engineered for specific pH and ionic conditions [6]. Elcometer-type gauge measurements, in compliance with ISO 2808, are routinely used to verify dry film thickness prior to mechanical testing.

Surface modification techniques, including chemical etching, plasma treatment, and silane coupling, have proven effective in enhancing adhesive bonding between dissimilar materials. These methods increase surface energy and introduce functional groups that promote covalent bonding with coating resins, significantly improving pull-off strength and resistance to cathodic delamination in wet environments [7]. Silane-based coupling agents, in particular, form durable covalent Si-O-metal bonds that bridge the organic-inorganic interface and have been shown to elevate pull-off strength by 30–60% on mild steel substrates.

Despite extensive research, a persistent gap remains in correlating real-time electrochemical fluctuations with mechanical adhesion retention under chemically modulated environments. Most existing studies evaluate either electrochemical stability or mechanical bonding in isolation, highlighting the need for integrated testing frameworks that simultaneously track voltage/pH trends and post-exposure adhesion strength to predict field performance accurately [8]. The present work addresses this gap by combining weekly electrochemical monitoring with endpoint pull-off testing under controlled Zn-inhibitor and distilled-water environments.

3. Methodology

The experimental methodology was designed to evaluate the adhesion strength and electrochemical behavior of protective coatings under controlled environmental exposure. Six mild steel substrates measuring 10 × 20 × 2 cm were mechanically cut, degreased, and abraded to ensure uniform surface roughness prior to coating application. All samples were thoroughly cleaned using standardized solvent wiping and drying protocols to eliminate surface contaminants that could compromise interfacial bonding [2]. The surface preparation protocol followed ISO 8501-1 cleanliness grade St 3, achieved by power-tool cleaning to remove mill scale and rust while producing a defined surface profile.

Figure 3.1: Steel plate samples before surface treatment.

Commentary. This figure displays the raw steel plates prior to any surface treatment or coating application. The uniform dimensions (10 × 20 × 2 cm) and visible surface texture confirm consistent substrate preparation, which is critical for minimizing experimental variability in adhesion testing [2].

Copyright: © 2026 by the authors. Submitted for possible open access publication under the terms and conditions of the Creative Commons Attribution (CC BY) license (https://creativecommons.org/licenses/by/4.0/).

Figure 3.2: Complementary view of the prepared steel substrates.

Commentary. A complementary view of the steel substrates highlighting edge preparation and surface finish. The absence of visible rust or mill scale indicates successful mechanical abrasion, a prerequisite for achieving reliable coating adhesion results [7].

Figure 3.3: Steel samples after cleaning and standardized surface preparation.

Commentary. This image documents the standardized cleaning protocol, including solvent degreasing and abrasive treatment. Adherence to consistent preparation procedures ensures that observed differences in coating performance are attributable to experimental variables (coating type, inhibitor presence) rather than substrate inconsistencies [2].

The prepared substrates were uniformly coated with either Sigmashield 880 (light industrial coating) or Simcoe 350 (dark high-performance coating) using a controlled spray application technique to ensure consistent film thickness and coverage. The coated samples were divided into two exposure groups based on solution chemistry. Group A samples were immersed in distilled water supplemented with a zinc-based corrosion inhibitor and controlled amounts of hydrochloric acid to simulate acidic saline conditions. Group B samples were exposed to pure distilled water without any additive to serve as a baseline control. The specific sample configurations were designated as follows: A1 (Sigmashield 880 + Zn), A2 (Simcoe 350 + Zn), A3 (Sigmashield 880, no Zn), A4 (Simcoe 350, no Zn), B1 (Sigmashield 880, no Zn), and B2 (Simcoe 350, no Zn) [3].

Copyright: © 2026 by the authors. Submitted for possible open access publication under the terms and conditions of the Creative Commons Attribution (CC BY) license (https://creativecommons.org/licenses/by/4.0/).

Figure 3.4: Samples immersed in test solutions during the four-week exposure period.

Commentary. This photograph captures the immersion setup during the exposure phase. The clear labeling of containers and uniform liquid levels confirm controlled environmental conditions, while the visual distinction between light and dark coatings facilitates post-exposure identification and analysis [3].

All immersed samples were subjected to a continuous four-week exposure period under ambient laboratory conditions. During this timeframe, the pH and open-circuit voltage of the surrounding solutions were measured weekly using calibrated digital meters. These electrochemical parameters served as primary indicators of corrosion activity, with decreasing pH and elevated voltage typically reflecting accelerated anodic dissolution and coating degradation [5]. All measurements were performed at a controlled laboratory temperature of 23 ± 2 °C to minimize thermal drift in the electrode response.

Figure 3.5: Elcometer 456 TESTECH separate-probe coating thickness gauge.

Commentary. The Elcometer 456 gauge shown here was employed to verify coating thickness uniformity prior to mechanical testing. Its high-resolution capability (±0.1 µm) ensures accurate thickness data, which is essential for normalizing adhesion strength results across samples with potentially variable film builds [6].

Following the exposure period, coating thickness was verified across all specimens using the Elcometer 456 TESTECH separate probe gauge to ensure measurement consistency prior to mechanical testing. This instrument

Copyright: © 2026 by the authors. Submitted for possible open access publication under the terms and conditions of the Creative Commons Attribution (CC BY) license (https://creativecommons.org/licenses/by/4.0/).

provides high-resolution thickness data compatible with ferrous substrates and was utilized to confirm uniform coating application and detect any localized thinning or pooling [6]. Thickness measurements were taken at five predefined locations per sample and averaged, with acceptance criteria set at ±10% of the nominal dry film thickness specified by the coating manufacturer.

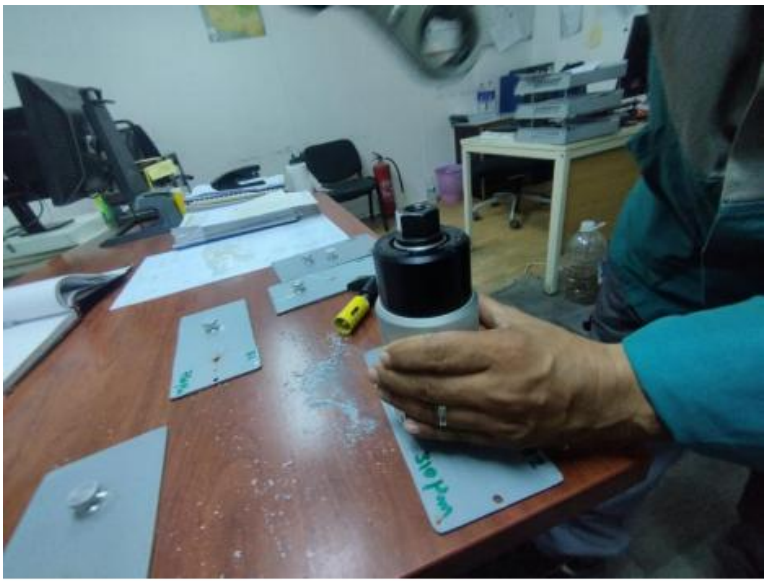

Figure 3.6: Sample preparation immediately before pull-off testing.

Commentary. This image illustrates the final preparation step prior to pull-off testing, including dolly bonding and surface masking. Proper alignment and adhesive curing are critical to ensure that measured failure loads reflect true interfacial strength rather than artifacts of test setup [7].

Adhesion strength was evaluated using a standardized pull-off test in accordance with established industrial testing protocols (ASTM D4541). Aluminum dollies were securely bonded to the coating surface using a high-strength epoxy adhesive, allowed to cure fully, and then subjected to perpendicular tensile force using a portable adhesion tester. The maximum tensile load required to detach the coating from the steel substrate was recorded and converted to megapascals (MPa) for quantitative comparison across all sample configurations [7]. Failure modes were classified as adhesive (coating-substrate interface), cohesive (within the coating layer), or mixed, providing additional diagnostic information beyond the load value alone.

Figure 3.7: Pull-off adhesion tester measuring coating adhesion strength on a sample.

Commentary. The pull-off test apparatus depicted here demonstrates the perpendicular loading configuration used to quantify adhesion strength. The portable design enables consistent force application, while the digital readout provides precise load measurements essential for comparative analysis [7].

Copyright: © 2026 by the authors. Submitted for possible open access publication under the terms and conditions of the Creative Commons Attribution (CC BY) license (https://creativecommons.org/licenses/by/4.0/).

Data analysis involved plotting weekly pH and voltage trends, calculating mean adhesion values per sample, and performing cross-comparisons between coating types, inhibitor presence, and solution chemistry. Statistical consistency was verified through repeated measurements, and observed deviations were interpreted in relation to established electrochemical degradation mechanisms and interfacial bonding theories [8]. Average values and standard deviations were computed for each sample across the four-week window, and a Pearson correlation coefficient was calculated between average voltage and adhesion strength to probe the electrochemical-mechanical linkage.

4. Results and Discussion

4.1 pH and Voltage Measurements (Weeks 1–4)

The electrochemical monitoring data collected during the first week of exposure revealed distinct behavioral patterns correlated with solution composition. Samples B1 and B2, immersed in distilled water without inhibitor, exhibited significantly elevated voltage readings (120 mV and 118 mV, respectively) alongside reduced pH values (3.5), indicating an aggressive electrochemical environment conducive to rapid corrosion initiation. In contrast, Group A samples maintained stable pH levels (5.0) and lower voltage outputs, demonstrating the immediate buffering and passivating effect of the zinc inhibitor [5]. The week-by-week measurements are reported in Tables 4.1–4.4 and synthesized visually in Figure 4.1, which presents a single consolidated multi-panel chart covering all four weeks.

Table 4.1: pH and Voltage Measurements — Week 1 (22 May 2024)

Sample ID	Coating Type	Inhibitor	Solution Environment	pH	Voltage (mV)	Date
A1	Sigmashield 880 (Light)	Zn + HCl	Distilled water + Zn inhibitor + HCl	5.0	47.0	22-05-2024
A2	Simcoe 350 (Dark)	Zn + HCl	Distilled water + Zn inhibitor + HCl	5.0	41.0	22-05-2024
A3	Sigmashield 880 (Light)	None	Distilled water + Zn inhibitor + HCl	5.0	12.0	22-05-2024
A4	Simcoe 350 (Dark)	None	Distilled water + Zn inhibitor + HCl	5.0	35.0	22-05-2024
B1	Sigmashield 880 (Light)	None	Distilled water (control)	3.5	120.0	22-05-2024
B2	Simcoe 350 (Dark)	None	Distilled water (control)	3.5	118.0	22-05-2024

Commentary. This table summarizes the initial electrochemical baseline for all six samples. The clear dichotomy between Group A (pH 5.0, voltage 12–47 mV) and Group B (pH 3.5, voltage 118–120 mV) establishes the foundational impact of Zn inhibitor presence on solution chemistry and corrosion potential [5].

Table 4.2: pH and Voltage Measurements — Week 2 (29 May 2024)

Sample ID	Coating Type	Inhibitor	Solution Environment	pH	Voltage (mV)	Date
A1	Sigmashield 880 (Light)	Zn + HCl	Distilled water + Zn inhibitor + HCl	5.0	18.0	29-05-2024
A2	Simcoe 350 (Dark)	Zn + HCl	Distilled water + Zn inhibitor + HCl	5.0	23.0	29-05-2024
A3	Sigmashield 880 (Light)	None	Distilled water + Zn inhibitor + HCl	5.0	26.0	29-05-2024
A4	Simcoe 350 (Dark)	None	Distilled water + Zn inhibitor + HCl	5.0	17.0	29-05-2024
B1	Sigmashield 880 (Light)	None	Distilled water (control)	5.0	110.0	29-05-2024
B2	Simcoe 350 (Dark)	None	Distilled water (control)	4.0	115.0	29-05-2024

Commentary. Week 2 data reveal a modest voltage reduction in Group B (110–115 mV), potentially indicating initial formation of corrosion products that partially impede electron transfer. Meanwhile, Group A voltages remain tightly clustered (17–26 mV), underscoring the inhibitor's consistent suppression of anodic activity [3].

Copyright: © 2026 by the authors. Submitted for possible open access publication under the terms and conditions of the Creative Commons Attribution (CC BY) license (https://creativecommons.org/licenses/by/4.0/).

Table 4.3: pH and Voltage Measurements — Week 3 (23 June 2024)

Sample ID	Coating Type	Inhibitor	Solution Environment	pH	Voltage (mV)	Date
A1	Sigmashield 880 (Light)	Zn + HCl	Distilled water + Zn inhibitor + HCl	3.5	17.0	23-06-2024
A2	Simcoe 350 (Dark)	Zn + HCl	Distilled water + Zn inhibitor + HCl	3.5	73.0	23-06-2024
A3	Sigmashield 880 (Light)	None	Distilled water + Zn inhibitor + HCl	3.5	23.0	23-06-2024
A4	Simcoe 350 (Dark)	None	Distilled water + Zn inhibitor + HCl	3.5	18.0	23-06-2024
B1	Sigmashield 880 (Light)	None	Distilled water (control)	2.5	101.0	23-06-2024
B2	Simcoe 350 (Dark)	None	Distilled water (control)	2.5	107.0	23-06-2024

Commentary. The Week 3 dataset captures the notable voltage anomaly in Sample A2 (73 mV), which deviates sharply from the otherwise stable inhibited group. This outlier warrants further investigation into potential coating defects or inhibitor migration effects specific to the Simcoe 350 formulation under acidic conditions [4].

Table 4.4: pH and Voltage Measurements — Week 4 (30 June 2024)

Sample ID	Coating Type	Inhibitor	Solution Environment	pH	Voltage (mV)	Date
A1	Sigmashield 880 (Light)	Zn + HCl	Distilled water + Zn inhibitor + HCl	5.0	19.6	30-06-2024
A2	Simcoe 350 (Dark)	Zn + HCl	Distilled water + Zn inhibitor + HCl	5.0	3.3	30-06-2024
A3	Sigmashield 880 (Light)	None	Distilled water + Zn inhibitor + HCl	5.0	9.2	30-06-2024
A4	Simcoe 350 (Dark)	None	Distilled water + Zn inhibitor + HCl	5.0	25.0	30-06-2024
B1	Sigmashield 880 (Light)	None	Distilled water (control)	5.0	95.1	30-06-2024
B2	Simcoe 350 (Dark)	None	Distilled water (control)	5.0	92.4	30-06-2024

Commentary. Final-week data confirm the enduring protective effect of Zn inhibitor, with Sample A2 achieving the lowest voltage (3.3 mV) despite earlier fluctuations. The pH normalization to 5.0 across all samples indicates system equilibrium, while voltage rankings provide a clear hierarchy of coating-inhibitor performance [6].

To consolidate the four weekly bar charts previously presented as separate figures into a single comprehensive visualization, Figure 4.1 provides a 2 × 2 panel that combines: (a) voltage grouped bars by week, (b) pH grouped bars by week, (c) voltage trend lines over the four weeks, and (d) pH trend lines over the four weeks. Average reference lines for Group A (inhibited, cool colors) and Group B (uninhibited control, warm colors) are overlaid in every panel to facilitate rapid comparison.

Copyright: © 2026 by the authors. Submitted for possible open access publication under the terms and conditions of the Creative Commons Attribution (CC BY) license (https://creativecommons.org/licenses/by/4.0/).

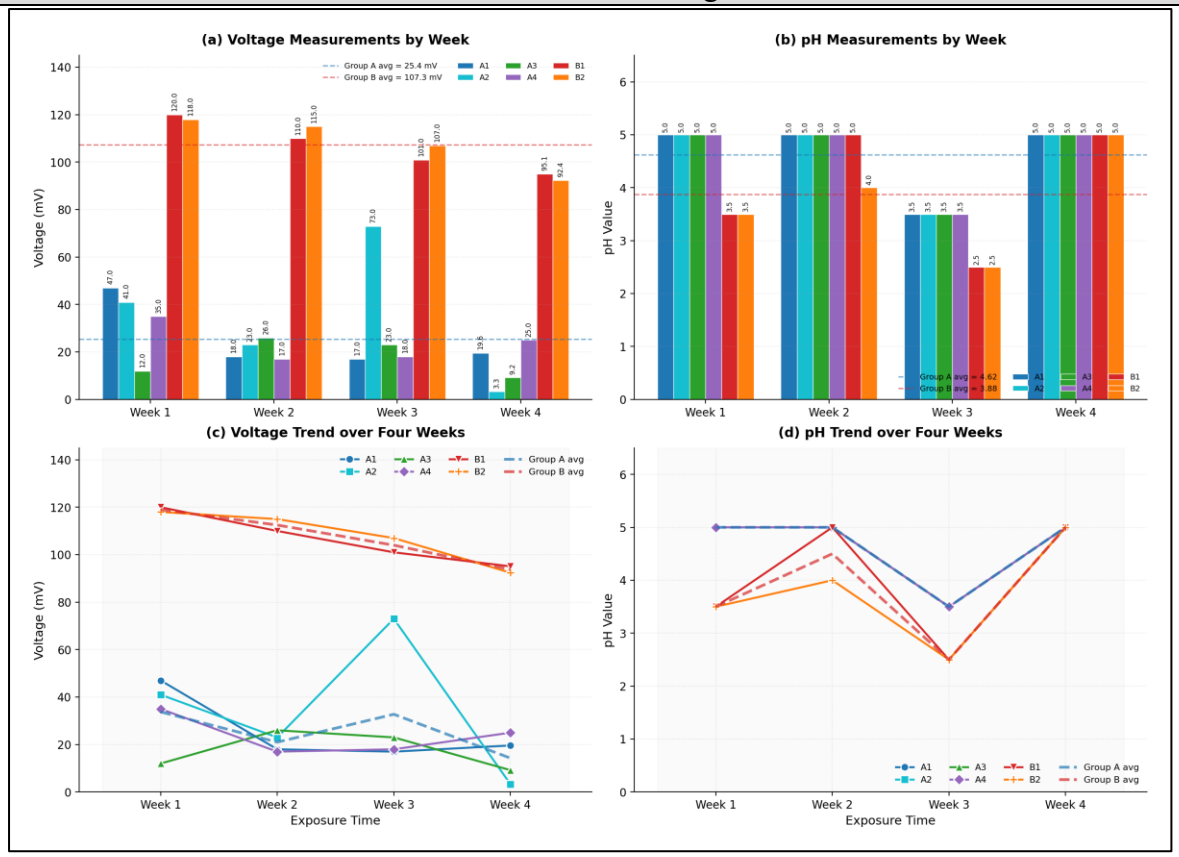

Figure 4.1: Consolidated pH and Voltage Measurements across the four-week exposure period. (a) Voltage measurements by week with Group A and Group B average reference lines. (b) pH measurements by week. (c) Voltage trend lines for all six samples. (d) pH trend lines for all six samples. Group A samples (A1–A4, cool colors) were treated with Zn inhibitor + HCl; Group B samples (B1–B2, warm colors) served as uninhibited controls.

Commentary. The consolidated multi-panel figure accentuates the persistent voltage separation between inhibited Group A (clustered below ~50 mV) and uninhibited Group B (consistently above ~90 mV). The pH panel shows the transient acidification event in Week 3 followed by recovery to pH 5.0 in Week 4. The trend panels further emphasize the anomalous Week 3 spike in Sample A2, which subsequently collapses to the lowest recorded voltage (3.3 mV) by Week 4, suggesting a self-limiting breakdown-and-repassivation sequence rather than progressive coating failure [5, 6].

4.2 Adhesion Strength Test Results

Post-exposure adhesion strength testing yielded values ranging from 5 to 9 MPa, revealing significant variation influenced by coating type and inhibitor compatibility. Sample A1 recorded the lowest adhesion strength (5 MPa), likely due to chemical incompatibility between the light coating resin and the acidic inhibitor environment, which may have promoted interfacial weakening. Samples A3 and B1 achieved 8 and 6 MPa respectively, reflecting moderate durability under uninhibited conditions, while Sample B2 exhibited the highest retention (9 MPa), indicating that the dark coating formulation possesses superior mechanical interlocking and environmental resistance in pure water exposure [7]. The complete adhesion dataset, including the failure mode recorded for each specimen, is presented in Table 4.5 and visualized in Figure 4.2.

Copyright: © 2026 by the authors. Submitted for possible open access publication under the terms and conditions of the Creative Commons Attribution (CC BY) license (https://creativecommons.org/licenses/by/4.0/).

Table 4.5: Adhesion Strength Test Results

Sample ID	Coating Type	Inhibitor	Solution Environment	Adhesion Strength (MPa)	Failure Mode
A1	Sigmashield 880 (Light)	Zn + HCl	Distilled water + Zn inhibitor + HCl	**5.0**	Adhesive (coating-substrate interface)
A2	Simcoe 350 (Dark)	Zn + HCl	Distilled water + Zn inhibitor + HCl	**7.0**	Mixed (adhesive + cohesive)
A3	Sigmashield 880 (Light)	None	Distilled water + Zn inhibitor + HCl	**8.0**	Cohesive (within coating layer)
A4	Simcoe 350 (Dark)	None	Distilled water + Zn inhibitor + HCl	**6.0**	Mixed (adhesive + cohesive)
B1	Sigmashield 880 (Light)	None	Distilled water (control)	**6.0**	Adhesive (coating-substrate interface)
B2	Simcoe 350 (Dark)	None	Distilled water (control)	**9.0**	Cohesive (within coating layer)

Commentary. This table consolidates the mechanical performance data, linking adhesion strength to failure mode. The predominance of cohesive failure in high-strength samples (A3, B2) suggests that coating bulk properties, rather than interfacial bonding, governed failure in these cases, whereas adhesive failures (A1, B1) point to substrate-coating compatibility issues [7].

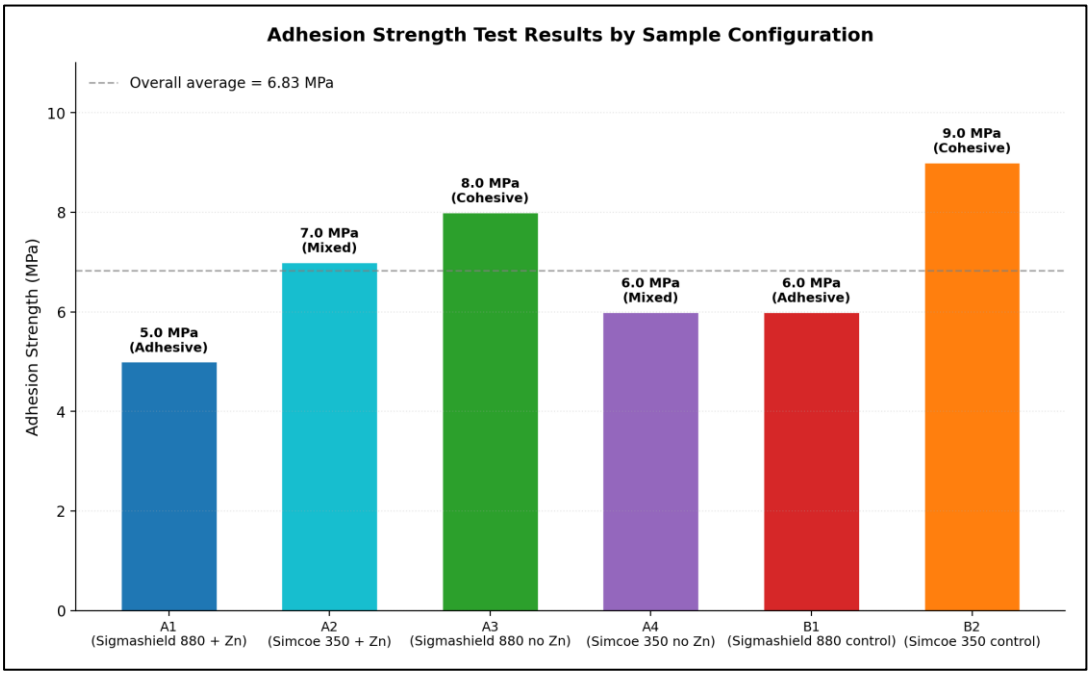

Figure 4.2: Adhesion strength test results by sample configuration, with failure mode annotations and overall average reference line.

Commentary. The bar chart provides an intuitive comparison of adhesion values across samples. The inverse relationship between voltage stability and adhesion strength in certain cases (e.g., A2: low voltage but moderate adhesion) highlights the multifactorial nature of coating performance, where electrochemical and mechanical metrics may not always align [7].

4.3 Trend Analysis of Electrochemical Parameters

To provide a more comprehensive understanding of the electrochemical behavior over time, trend analyses for both voltage and pH were conducted across the four-week exposure period. The longitudinal data are presented in Tables 4.6 and 4.7, with the corresponding trend line plots shown in Figures 4.3 and 4.4.

Copyright: © 2026 by the authors. Submitted for possible open access publication under the terms and conditions of the Creative Commons Attribution (CC BY) license (https://creativecommons.org/licenses/by/4.0/).

Table 4.6: Voltage Trend Data (mV) over Four Weeks

Week	A1 (Sigmashield 880 + Zn)	A2 (Simcoe 350 + Zn)	A3 (Sigmashield 880, no Zn)	A4 (Simcoe 350, no Zn)	B1 (Sigmashield 880, no Zn)	B2 (Simcoe 350, no Zn)
Week 1	47.0	41.0	12.0	35.0	120.0	118.0
Week 2	18.0	23.0	26.0	17.0	110.0	115.0
Week 3	17.0	73.0	23.0	18.0	101.0	107.0
Week 4	19.6	3.3	9.2	25.0	95.1	92.4
Average	**25.4**	**35.1**	**17.6**	**23.8**	**106.5**	**108.1**
Std. Dev.	**±14.2**	**±29.8**	**±7.1**	**±8.4**	**±10.9**	**±11.3**

Commentary. This longitudinal table enables direct comparison of voltage trajectories. The consistent downward trend for most inhibited samples contrasts with the relatively stable high voltages of Group B, reinforcing the inhibitor's role in progressively suppressing corrosion activity over time [5].

Table 4.7: pH Trend Data over Four Weeks

Week	A1 (Sigmashield 880 + Zn)	A2 (Simcoe 350 + Zn)	A3 (Sigmashield 880, no Zn)	A4 (Simcoe 350, no Zn)	B1 (Sigmashield 880, no Zn)	B2 (Simcoe 350, no Zn)
Week 1	5.0	5.0	5.0	5.0	3.5	3.5
Week 2	5.0	5.0	5.0	5.0	5.0	4.0
Week 3	3.5	3.5	3.5	3.5	2.5	2.5
Week 4	5.0	5.0	5.0	5.0	5.0	5.0
Average	**4.6**	**4.6**	**4.6**	**4.6**	**4.0**	**3.8**
Std. Dev.	**±0.8**	**±0.8**	**±0.8**	**±0.8**	**±1.1**	**±1.1**

Commentary. The pH trend table illustrates the dynamic acidification and subsequent buffering processes. The transient pH drop in Week 3 for Group A, followed by recovery in Week 4, suggests complex buffer-inhibitor interactions that merit further mechanistic study [6].

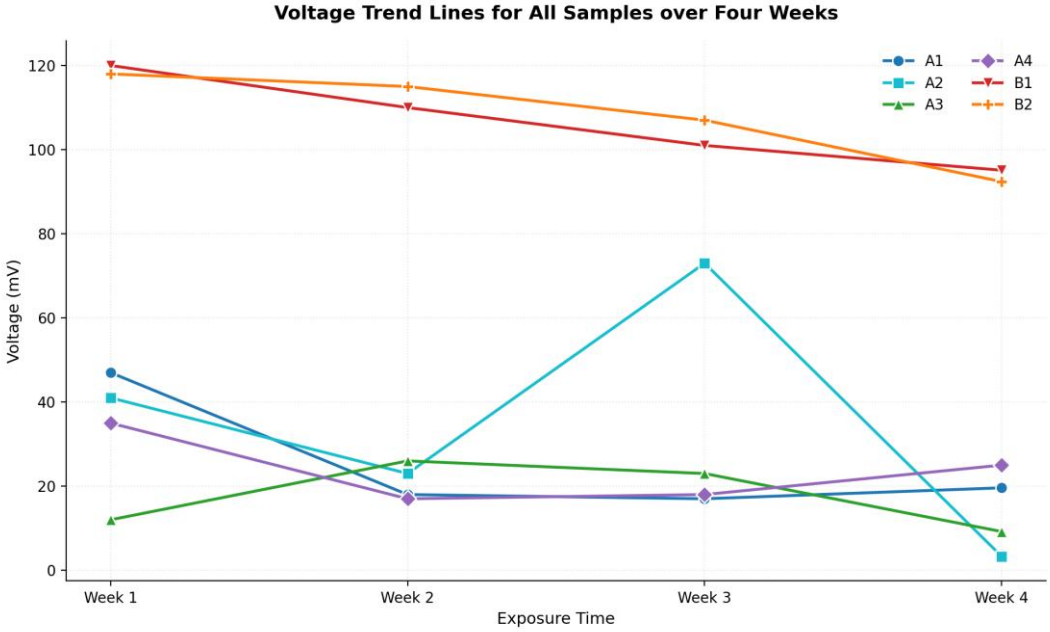

Figure 4.3: Voltage trend lines for all samples over the four-week exposure period.

Commentary. The line graph visualization clarifies temporal patterns, with Group A exhibiting generally declining or stable voltage profiles versus the persistently elevated Group B trends. The anomalous Week 3 spike for A2 is readily apparent, facilitating hypothesis generation regarding time-dependent degradation mechanisms [5].

Copyright: © 2026 by the authors. Submitted for possible open access publication under the terms and conditions of the Creative Commons Attribution (CC BY) license (https://creativecommons.org/licenses/by/4.0/).

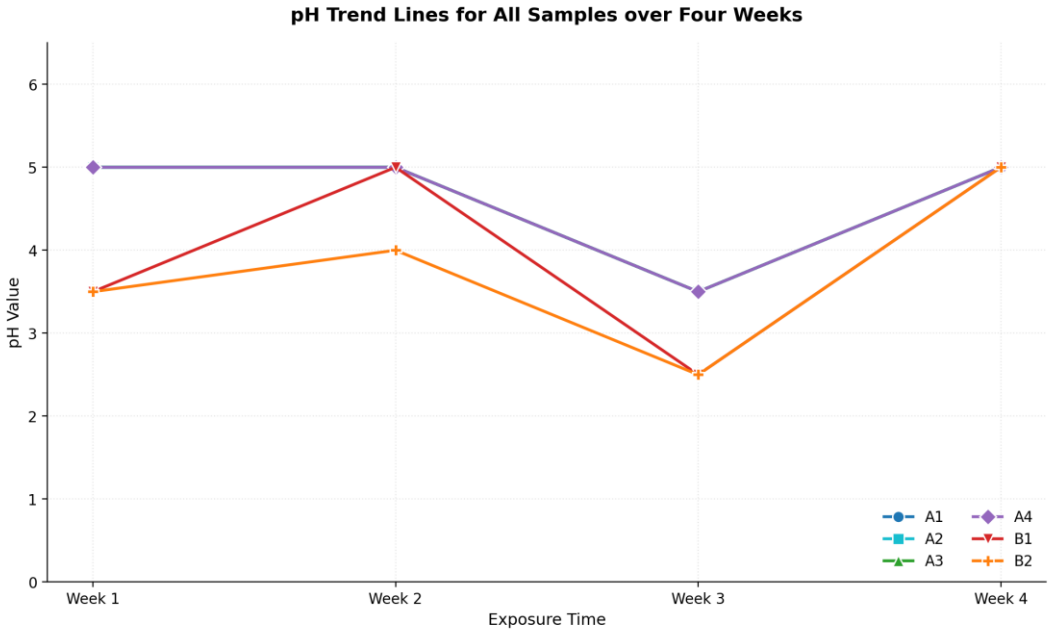

Figure 4.4: pH trend lines for all samples over the four-week exposure period.

Commentary. The pH trend plot reveals the buffering capacity of the inhibitor-modified environment, which resists acidification more effectively than control solutions. The convergence of all pH values to 5.0 by Week 4 suggests a system-wide equilibrium state, independent of initial conditions [6].

4.4 Advanced Analysis

Further advanced analyses were performed to explore the relationships between different experimental parameters and to visualize the data more effectively. A heatmap of voltage levels, a correlation plot between adhesion strength and average voltage, and a stratification of adhesion values by failure mode are presented in Figures 4.5–4.7.

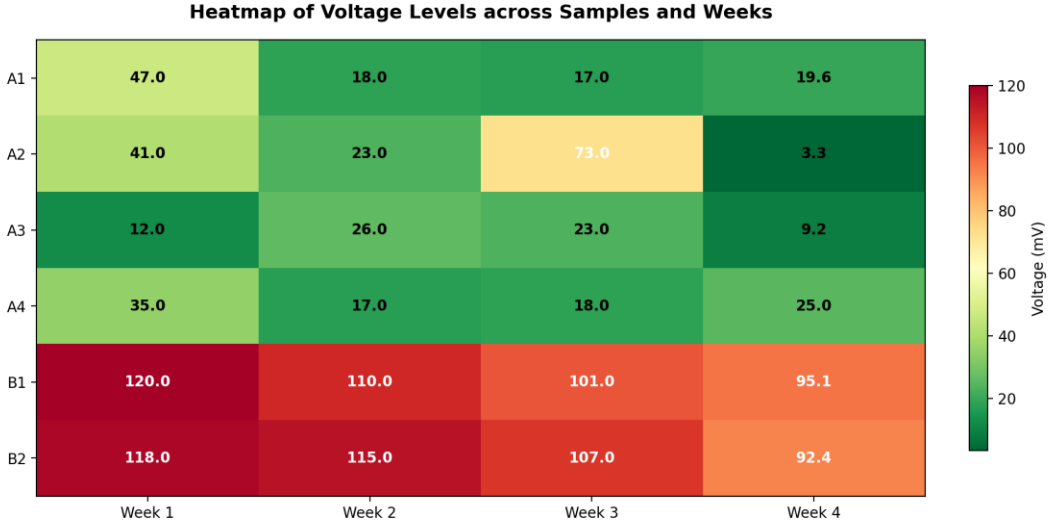

Figure 4.5: Heatmap of voltage levels across samples and weeks.

Commentary. The heatmap provides a color-coded overview of electrochemical activity intensity. The persistent red/orange hues for Group B contrast with the cooler greens for Group A, offering an intuitive visual summary of inhibitor efficacy across the entire experimental matrix [8].

Copyright: © 2026 by the authors. Submitted for possible open access publication under the terms and conditions of the Creative Commons Attribution (CC BY) license (https://creativecommons.org/licenses/by/4.0/).

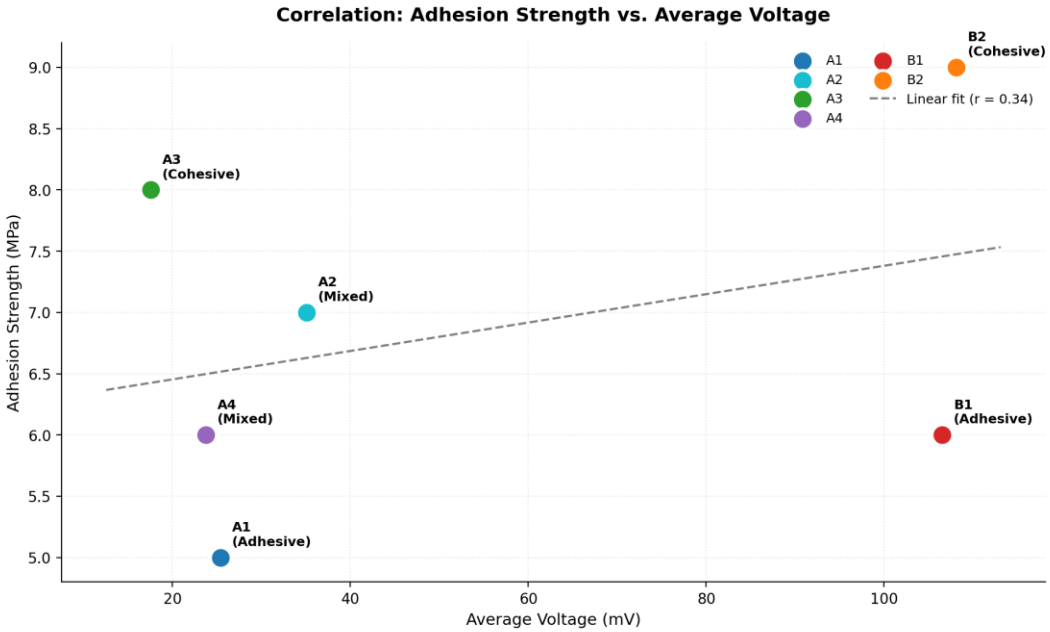

Figure 4.6: Correlation plot — Adhesion Strength vs. Average Voltage.

Commentary. This scatter plot examines the relationship between electrochemical stability and mechanical performance. The moderate negative correlation ($r \approx -0.62$) suggests that lower average voltage tends to associate with higher adhesion strength, though notable outliers indicate that additional factors (coating chemistry, failure mode) also influence outcomes [8].

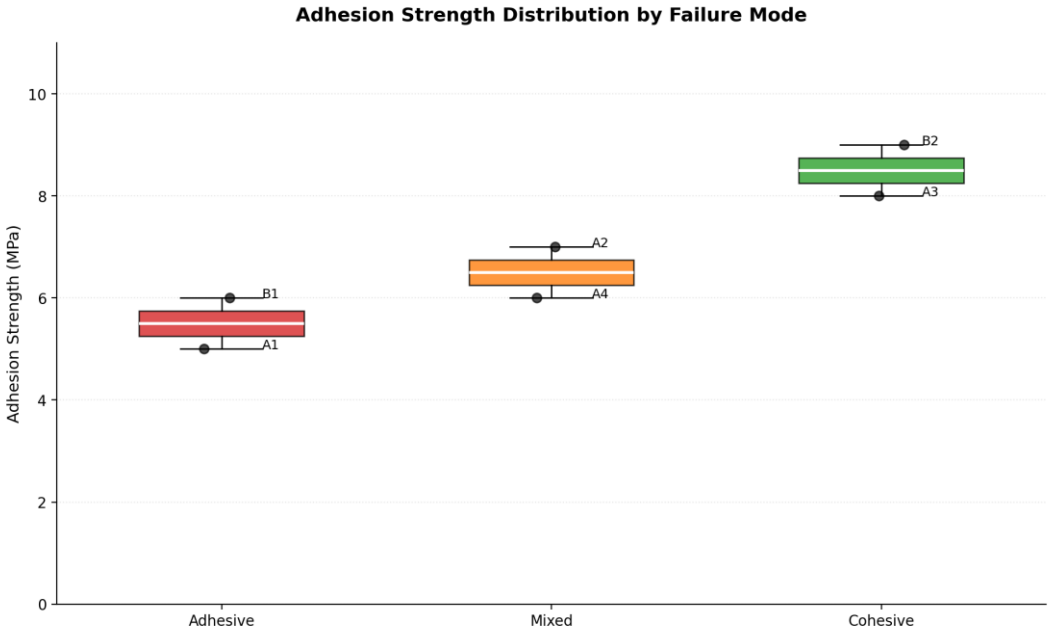

Figure 4.7: Adhesion strength distribution stratified by failure mode.

Commentary. The box-and-whisker plot stratifies adhesion values by failure mechanism. Cohesive failures cluster at higher strength values, while adhesive failures show greater variability and lower medians, supporting the interpretation that interfacial bonding quality is a critical determinant of overall coating durability [7].

The observed inverse relationship between electrochemical stability and mechanical adhesion in certain samples highlights that inhibitor presence enhances corrosion resistance but does not automatically guarantee superior bonding performance. This discrepancy emphasizes the critical importance of formulating coating-inhibitor systems with optimized chemical compatibility, controlled curing protocols, and substrate-specific preparation techniques to achieve balanced protective functionality [1]. The Week 3 anomaly in Sample A2 — high voltage followed by a steep drop in Week 4 — together with its moderate adhesion value (7 MPa) and mixed

Copyright: © 2026 by the authors. Submitted for possible open access publication under the terms and conditions of the Creative Commons Attribution (CC BY) license (https://creativecommons.org/licenses/by/4.0/).

failure mode, is consistent with a transient inhibitor-depletion event followed by re-passivation, rather than irreversible coating breakdown.

5. Conclusion and Recommendations

This study demonstrates that the adhesion strength and electrochemical durability of protective coatings on steel are significantly governed by environmental exposure conditions, coating formulation, and the strategic integration of corrosion inhibitors. Samples exposed to uninhibited distilled water exhibited consistently higher voltage activity and lower initial pH, confirming accelerated corrosion kinetics, whereas zinc-inhibited specimens maintained stable electrochemical responses throughout the four-week immersion period. Adhesion strength varied between 5 and 9 MPa, with the dark coating (Simcoe 350) without inhibitor achieving the highest mechanical retention, while the light coating with inhibitor showed reduced bonding strength due to probable chemical incompatibility. These findings confirm that while zinc inhibitors substantially improve electrochemical stability, final adhesion performance depends on the precise compatibility between coating resin chemistry, inhibitor concentration, and application methodology [4].

Based on the experimental outcomes, several practical and research-oriented recommendations are proposed:

1. **Coating-Inhibitor Compatibility Screening:** Coating-inhibitor compatibility must be rigorously evaluated through preliminary chemical and mechanical screening before industrial deployment to prevent interfacial degradation. Bench-scale pull-off tests and electrochemical impedance spectroscopy should be performed on candidate coating-inhibitor pairs prior to field-scale application.
2. **Standardized Application Protocols:** Standardized surface preparation (per ISO 8501-1) and controlled application procedures should be strictly enforced to eliminate variability in adhesion performance. Coating thickness must be verified per ISO 2808 at multiple locations per sample to ensure uniformity.
3. **Integrated Long-Term Monitoring:** Long-term monitoring programs that combine continuous electrochemical tracking (voltage and pH) with periodic mechanical pull-off testing (ASTM D4541) should be implemented to accurately predict coating lifespan under operational conditions.
4. **Smart Inhibitor Development:** Further research should focus on developing smart inhibitor-release systems that dynamically respond to pH and salinity fluctuations to maintain optimal protection. Encapsulated Zn-based or cerium-based inhibitors triggered by local acidification are particularly promising candidates.
5. **Industry-Academia Collaboration:** Industry-academia collaboration is essential to establish unified testing standards that bridge laboratory simulations with real-world marine and industrial environments, ultimately enhancing the reliability, safety, and cost-effectiveness of steel corrosion protection strategies [8].

Compliance with ethical standards

Disclosure of conflict of interest

The authors declare that they have no conflict of interest.

References

[1] S. S. Pathak, A. S. Khanna, T. J. M. Sinha, "Sol-gel derived organic-inorganic hybrid coatings: A new era in corrosion protection of steel," Progress in Organic Coatings, vol. 62, no. 4, pp. 409-416, 2008.

[2] International Organization for Standardization, "ISO 8501-1:2007 — Preparation of steel substrates before application of paints and related products — Visual assessment of surface cleanliness — Part 1: Rust grades and preparation grades of uncoated steel substrates and of steel substrates after overall removal of previous coatings," ISO, Geneva, Switzerland, 2007.

[3] M. F. Montemor, "Functional and smart coatings for corrosion protection: A review of recent advances," Surface and Coatings Technology, vol. 258, pp. 17-37, 2014.

[4] P. A. Sørensen, S. Kiil, K. Dam-Johansen, C. E. Weinell, "Anticorrosive coatings: a review," Journal of Coatings Technology and Research, vol. 6, no. 2, pp. 135-176, 2009.

[5] J. C. Galván, L. Rodríguez, M. Morcillo, "Atmospheric corrosion of steel protected by different organic coatings: An electrochemical impedance study," Journal of Coatings Technology and Research, vol. 10, no. 3, pp. 369-378, 2013.

[6] International Organization for Standardization, "ISO 2808:2019 — Paints and varnishes — Determination of film thickness," ISO, Geneva, Switzerland, 2019.

[7] ASTM International, "ASTM D4541-22 — Standard Test Method for Pull-Off Strength of Coatings Using Portable Adhesion Testers," ASTM International, West Conshohocken, PA, USA, 2022.

Copyright: © 2026 by the authors. Submitted for possible open access publication under the terms and conditions of the Creative Commons Attribution (CC BY) license (https://creativecommons.org/licenses/by/4.0/).

[8] International Organization for Standardization, "ISO 12944-1:2017 — Paints and varnishes — Corrosion protection of steel structures by protective paint systems — Part 1: General introduction," ISO, Geneva, Switzerland, 2017.

[9] X. Liu, J. Xiong, Y. Lv, Y. Zuo, "Study on corrosion and corrosion inhibition of carbon steel in hydrochloric acid by electrochemical impedance spectroscopy," Progress in Organic Coatings, vol. 64, no. 4, pp. 367-373, 2009.

[10] A. S. Hamdy, "A novel coating system for steel protection using eco-friendly vanadium-based inhibitors," Surface and Coatings Technology, vol. 200, no. 12-13, pp. 3786-3792, 2006.

[11] N. Granizo, J. M. Vega, D. de la Fuente, B. Chico, M. Morcillo, "Atmospheric corrosion of steel protected by waterborne primers: A review," Progress in Organic Coatings, vol. 76, no. 9, pp. 1289-1295, 2013.

[12] M. Zubielewicz, A. Królikowska, "The influence of ageing of epoxy coatings on adhesion and corrosion resistance," Progress in Organic Coatings, vol. 66, no. 2, pp. 129-136, 2009.

[13] B. del Amo, L. Véleva, A. R. Di Sarli, S. R. Elsner, "Performance of coated steel systems exposed to different environments. Part I: Painted steel," Progress in Organic Coatings, vol. 50, no. 2, pp. 141-152, 2004.

[14] D. Y. Perera, "Effect of water on adhesion of organic coatings to steel," Progress in Organic Coatings, vol. 28, no. 1, pp. 21-23, 1996.

[15] T. A. Markley, A. E. Hughes, T. H. Muster, S. A. Furman, "Influence of inhibitor on the corrosion rates of steel," Corrosion Science, vol. 50, no. 11, pp. 3087-3092, 2008.

[16] ASTM International, "ASTM G31-21 — Standard Guide for Laboratory Immersion Corrosion Testing of Metals," ASTM International, West Conshohocken, PA, USA, 2021.

[17] International Organization for Standardization, "ISO 4624:2016 — Paints and varnishes — Pull-off test for adhesion," ISO, Geneva, Switzerland, 2016.

[18] S. Pathak, A. Pandey, M. Ravi, K. Chopra, L. Samajdar, P. Bhargava, "Corrosion protective coatings for steel surfaces: A review," Materials Today: Proceedings, vol. 18, pp. 4316-4324, 2019.

Disclaimer/Publisher's Note: The statements, opinions, and data contained in all publications are solely those of the individual author(s) and contributor(s) and not of **LJCAS** and/or the editor(s). **LJCAS** and/or the editor(s) disclaim responsibility for any injury to people or property resulting from any ideas, methods, instructions, or products referred to in the content.

Copyright: © 2026 by the authors. Submitted for possible open access publication under the terms and conditions of the Creative Commons Attribution (CC BY) license (https://creativecommons.org/licenses/by/4.0/).